Journal of the Australian Ceramic Society (2022) 58:1415–1421
https://doi.org/10.1007/s41779-022-00712-7

RESEARCH

Production of Zn-doped TiO_2 film with enhanced photocatalytic activity

Tuncay Dikici[1,2] · Ozan Yılmaz[3,4] · Alper Akalın[3] · Selim Demirci[5] · Serdar Gültekin[3] · Serdar Yıldırım[4] · Metin Yurddaşkal[4]

Received: 23 August 2021 / Revised: 4 January 2022 / Accepted: 6 February 2022 / Published online: 4 April 2022

Abstract

In this study, zinc (Zn)-doped titanium dioxide (TiO_2) films were prepared using the two steps: anodic oxidation method and heat treatment process. The crystal structure, morphology and elemental composition of the Zn-doped TiO_2 films were investigated. These films were characterized by scanning electron microscopy (SEM) with energy-dispersive spectroscopy (EDS), X-ray diffraction (XRD) and X-ray photoelectron spectroscopy (XPS). The results indicated that the TiO_2 films with clear, uniform and short nanopores had a high surface area and high degree of crystallinity. The results showed that the as-anodized TiO_2 film was successfully obtained as anatase phase at 450 °C. The results of XPS analysis confirmed the presence of Zn in the lattice of TiO_2 as dopant, and thermal diffusion technique was successfully done as doping method. The photocatalytic performances of the Zn-doped TiO_2 films were evaluated in terms of their photodegradation rate of methylene blue (MB) in an aqueous solution under UV light irradiation. The results revealed that the Zn-doped TiO_2 film had a higher photocatalytic activity in comparison with the undoped sample. This study inspired that Zn-doped TiO_2 films are a great potential material to treat wastewater in industrial field.

Keywords Zinc · TiO_2 films · XPS · Photocatalytic activity · Hydrothermal method

Introduction

TiO_2 is one of the most studying semiconducting materials. It has remarkably attractive properties such as nontoxicity, photoactivity and physically and chemically stability [1–4] which allow it to be used a wide range of application areas, such as air and water purifications, self-cleaning window glasses, lithium batteries, gas sensing, dielectric layer and solar cell [5–13]. Different methods have been tried to increase the efficiency and performance of TiO_2. Doping method is among the highlights of these studies. T. Umebayashi and his team have shown that S doping into the TiO_2 crystal lattice reduces the absorption line of titanium dioxide to a lower energy level [14]. S. Sakthivel et al. focused Pt, Au and Pd doped TiO_2 in their study. According to the results of this study, the light absorption of the doped samples in the visible region is higher than the non-doped ones. Furthermore they revealed that the higher dopant content caused increased level of absorption [15]. Among remarkable properties of TiO_2, it is noteworthy that especially water purification by the photocatalytic degradation reaction of TiO_2 is induced by UV light. Since Fujishima and Honda's research, many researcher have focused on the photocatalytic performance of TiO_2 [16].

Method of metal doping into host lattice commonly preferred technique to increase photocatalytic activity of TiO_2. Different studies revealed that doping Pt and Au can effectively suppress the electron–hole recombination by acting as an electron and/or hole traps [17, 18]. Another research showed that doping of Ag to TiO_2 lattice

✉ Serdar Gültekin
serdar.gultekin@deu.edu.tr

1 Torbali Vocational School, Dokuz Eylul University, Torbali, Izmir, Turkey

2 Center for Fabrication and Application of Electronic Materials, Dokuz Eylul University, Buca, 35390 Izmir, Turkey

3 The Graduate School of Natural and Applied Sciences, Dokuz Eylul University, Buca, Izmir, Turkey

4 Department of Metallurgical and Materials Engineering, Dokuz Eylul University, Buca, 35390 Izmir, Turkey

5 Department of Metallurgical and Materials Engineering, Marmara University, Kadiköy, 34722 Istanbul, Turkey

up to particular amount has remarkably positive effect on photodegrading performance of TiO_2 [13]. According to Marci and his team's research, increasing photocatalytic activity could be attributed to Zn content which increase in the separation rate of photo-induced charge due to the difference in the energy band position [19]. Different techniques have been used to doping process by researchers such as sol–gel, sputtering and liquid-phase precipitation [19–21]. However, these doping methods are complicated and require intense attention during process. In this study, we preferred thermal diffusion technique for doping process. Recent studies show us that the thermal diffusion technique can be employed to modify host material for different application such as boron doping of single crystal natural diamond, penetrating of indium to Cds film and germanium or tin doping in silicon [22–25]. One of the common expressions of these researches is simplicity and cost-effectiveness of the thermal diffusion technique. However, very few studies have focused on this technique for doping into photocatalytic host materials.

In this study, nanotubes were formed on Ti material by anodic oxidation of TiO_2. Then Zn doping process was carried out using thermal diffusion method in conventional furnace. In this way, doping and heat treatment process was completed at the same time. Zn was doped into TiO_2 for 2 h at 450 °C by thermal diffusion method. Morphological structure of the samples was characterized using scanning electron microscope (SEM), and elemental analysis was carried out with X-ray photoelectron spectroscopy and energy-dispersive spectroscopy (XPS and EDS). Crystal structures were investigated X-ray diffraction (XRD) technique. Photocatalytic performances were tested by measuring degradation rates and kinetic measurement.

Experimental studies

The substrate material of anodic oxidation was in the shape of a disc, 25 mm in diameter and 8-mm-thick pure Ti. The samples were polished incrementally with 120-grit to 2000-grit emery paper and then washed with acetone, ethanol and distilled water in an ultrasonic cleaner for 15 min. Before the experiment, the samples were etched in a mixture of nitric acid (HNO_3) and hydrofluoric acid (HF) solutions for 15 s to remove the naturally occurring oxide layer.

The electrochemical anodization was carried out at room temperature using a DC power supply. The experimental constant potential was 20 V for 30 min, and the distance between the anode and cathode was kept constant at 5 cm. A Ti sample was used as the anode. The electrolyte solution was stirred magnetically during the electrochemical reaction. After anodic oxidation, the as-anodized specimens were annealed at 450 °C for 2 h. Doping process was carried out by easily putting a Zn plate on the anodized titanium sample during heat treatment. The synthesis process mentioned above is also illustrated in Fig. 1.

The structural data of the samples were deduced from XRD (Thermo Scientific, ARL Kα) patterns with the help of a diffractometer with a CuK_α irradiation. Diffraction patterns were collected in the range of 10 to 90° with a scanning rate of 2°/min.

The morphology and elemental composition of the samples were characterized by a SEM (JEOL 6060) equipped with EDS analysis using samples without coating.

Surface chemistry of undoped and Zn-doped TiO_2 films was analysed through XPS (Thermo Scientific) with monochromatic Al-K_α (1486.7 eV) X-ray source and a beam size of 400 nm diameter. Calibration and analysis parameter of XPS system such as pass energy, resolution and gas purging were set as we did our previous study [26].

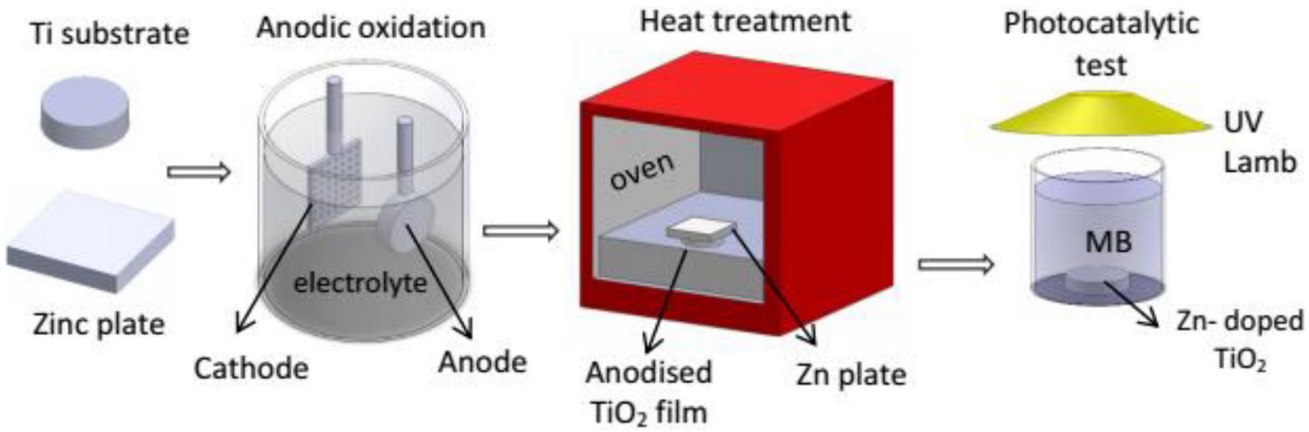

Fig. 1 Schematic representation for the synthesis of Zn-doped TiO_2 film by anodic oxidation method and heat treatment process

Photocatalytic performances of undoped and Zn-doped TiO_2 were examined by using the decolourization of the methylene blue (MB) aqueous solution. Photocatalytic activity experiments were carried out under a light source (Osram, Ultra Vitalux E27, 300 W) which emits both UV and visible light. The initial concentration of MB solution was 10^{-5} M. The pH value of the MB solution was 7.2. Then, the solutions were irradiated with light and taken for analysis at regular interval time. It was observed the absorbance values of the solutions via a UV–visible spectrophotometer (UV-1240 Shimadzu UV/VIS).

Results and discussion

XRD analysis

The XRD pattern of the prepared undoped and Zn-doped TiO_2 nanotubes was shown in Fig. 2. It can be seen in Fig. 1 that anatase phase formed for both sample after calcination according to XRD measurement. Metallic titanium was attributed from substrate sample. As can be seen from the XRD results, all peaks belong to Ti/TiO_2, and no peak was detected from the Zn or ZnO phases. The absence of Zn peaks in the XRD patterns is related to the low amount and small size.

Surface morphology of the samples

The surface morphology of the prepared TiO_2 nanotubes was depicted in Fig. 3. Figure 3a and b corresponded to undoped TiO_2 nanotube structure. It can be seen that the morphology of TiO_2 composed of tube structure which formed uniformly on the substrate. The diameter of the tubes was varying in the range of 50–100 nm. In addition, thickness of the TiO_2 was found to be approximately 250 nm from cross-sectional micrographs in Fig. 3a. Also, EDS spectra of surface was obtained in Fig. 3b. It should be noticed that the surface mainly consisted of Ti and O elements. Figure 3c belonged to Zn-doped TiO_2 nanolayer structure. The surface morphology of the Zn-doped TiO_2 layer was very similar to that of undoped TiO_2 layer. No differences between morphology of the samples were observed. Beside the morphology, EDX result confirmed that the layer consisted of Ti, Zn and O elements which means that Zn incorporation was succeeded.

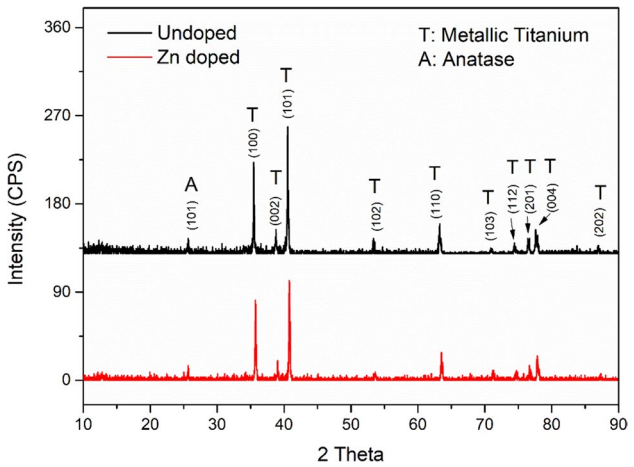

Fig. 2 XRD undoped TiO_2 nanotubes and Zn-doped TiO_2 nanotubes

XPS

The chemical composition, oxidation and the valence states of the various elements in the undoped and Zn-doped films were analysed using X-ray photoelectron spectroscopy, as shown in Fig. 4 which represents the results of the survey and high-resolution elemental scans of films. The binding energies of the existing elements and weight percentages of the analyses are exhibited in Table 1 in detail. Figure 4a shows the survey spectrum of the films. Ti 2p and O 1 s photoelectron peaks were observed at 459 and 531 eV, respectively, on the undoped TiO_2 sample. Zn-doped Zn 2p element was also detected at 1023 eV with Ti and O elements on the Zn-doped TiO_2 sample. As a result of the analyses, it was seen that Zn element was successfully diffused into the structure. In addition, no other elements were detected on both surfaces. As shown in Fig. 3d, the Zn element was determined as 0.34 wt% on EDS result, while it was observed that the XPS result was 44 wt% (Table 1) in the structure. This is because EDS receives data from the surface of the material at a depth of 1 µm, while XPS receives data from the surface of 1–10 nm. Therefore, the presence of Zn element in XPS is better observed in the structure.

Figure 4b–f shows the high-resolution XPS spectra of the Ti, O and Zn elements for both samples. Figure 4b–c depicts the deconvoluted spectrum of the Ti 2p element detected in the undoped and Zn-doped TiO_2 samples. In both spectra, 2 peaks were observed in almost the same binding energies. The peaks located at 465 and 459.4 eV can be assigned to Ti ($2p_{1/2}$) and Ti ($2p_{3/2}$), respectively. The splitting between both Ti ($2p_{1/2}$) and Ti ($2p_{3/2}$) core levels is observed around 5.7 eV, which is indicative of Ti^{4+} in the anatase phase of the TiO_2 film [27, 28]. In the Zn-doped film with low zinc concentration, the zinc sites also act as shallow electron trap to inhibit the recombination of photogenerated electrons and holes. In this way, the electron density of Ti^{4+} increases because the electron lifetime is prolonged. After the concentration of doped zinc reaches a proper value, the zinc sites become deep traps for electrons. Electron lifetime and density are reduced quickly in high zinc concentration films. For these reasons,

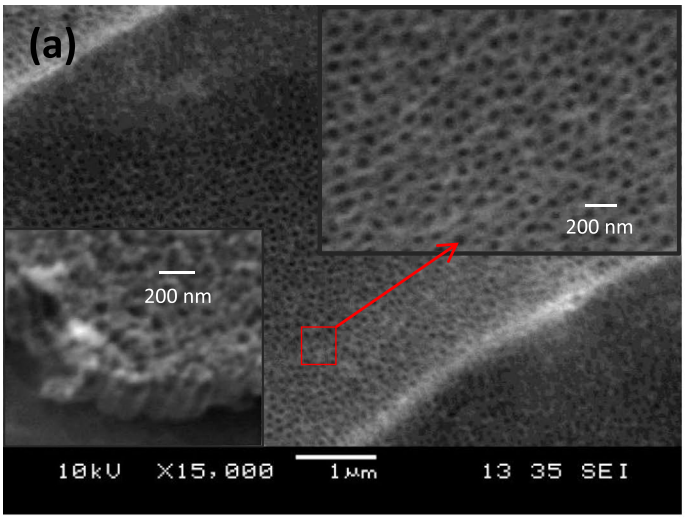

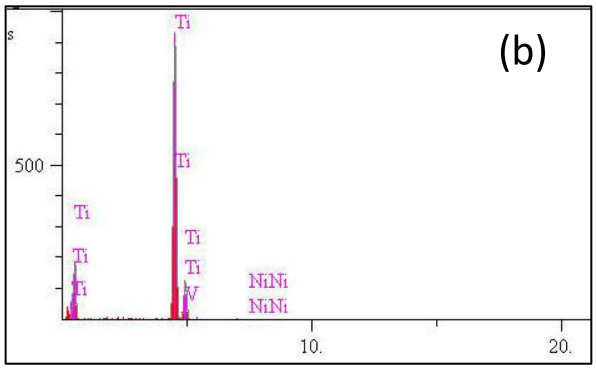

Element	Wt %
Ti	61.02
O	38.82
Other	0.16

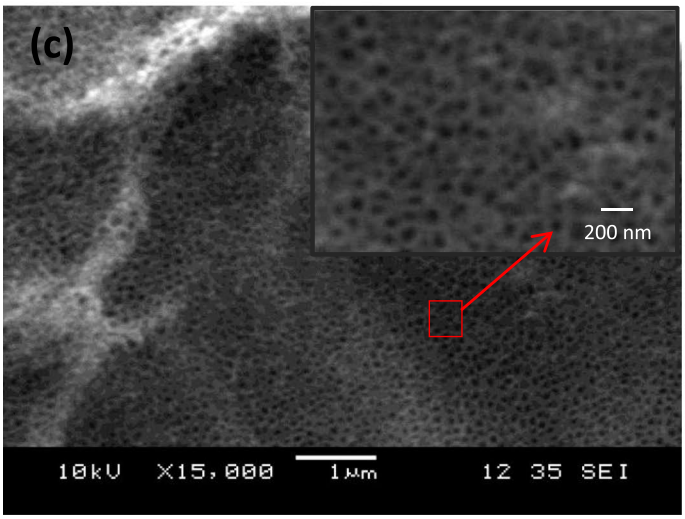

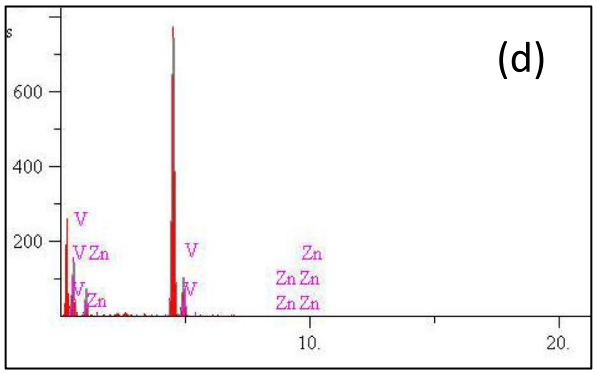

Element	Wt %
Ti	61.53
O	37.88
Zn	0.25
Other	0.34

Fig. 3 SEM images of **a**, **b** undoped TiO_2 nanotubes and **c**, **d** Zn-doped TiO_2 nanotubes

titanium oxidation state is only slightly influenced by the doped zinc oxide [21]. However, the reason for the low band shift in the Ti 2p peaks of undoped and Zn-doped TiO_2 is the formation of a large number of oxygen vacancies in the film structure after Zn doping. These oxygen vacancies cause the formation of Ti with lower valence. In addition, Zn^{2+} ions doping into the structure experience a slightly stronger pull from neighbouring Ti^{4+} ions with higher oxidation potential. This results in a slight increase in binding energy compared to the Zn^{2+} ion [29–31].

Figure 4d belongs to the photoelectron spectrum of the deconvoluted O 1 s of the undoped TiO_2 sample. The broad and asymmetric peaks indicate that there are at least two types of oxygen species on the surface. Fitting of the curves gives two components centred at 529.9 eV and 531.6 eV, which are assigned to lattice oxygen (O–Ti) and surface-bound hydroxyl groups (OHs), respectively [30, 32]. Similarly, two peaks were observed in the photoelectron spectrum of the Zn-doped TiO_2 sample given in Fig. 4e. These peaks belong to metal oxide and surface-bound hydroxyl groups. The binding energies of O 1 s belong to Zn-doped TiO_2 in Fig. 4e shifted toward the higher energy side compared to those of undoped TiO_2. Therefore, it can be assumed that Zn introduction affected the chemical states of TiO_2. XPS spectra of Zn 2p region are given in Fig. 4f. Zn ($2p_{3/2}$, $2p_{1/2}$) doublet was observed at 1022.69 eV and 1045.8 eV, indicating Zn in 2 + state bonding with oxygen

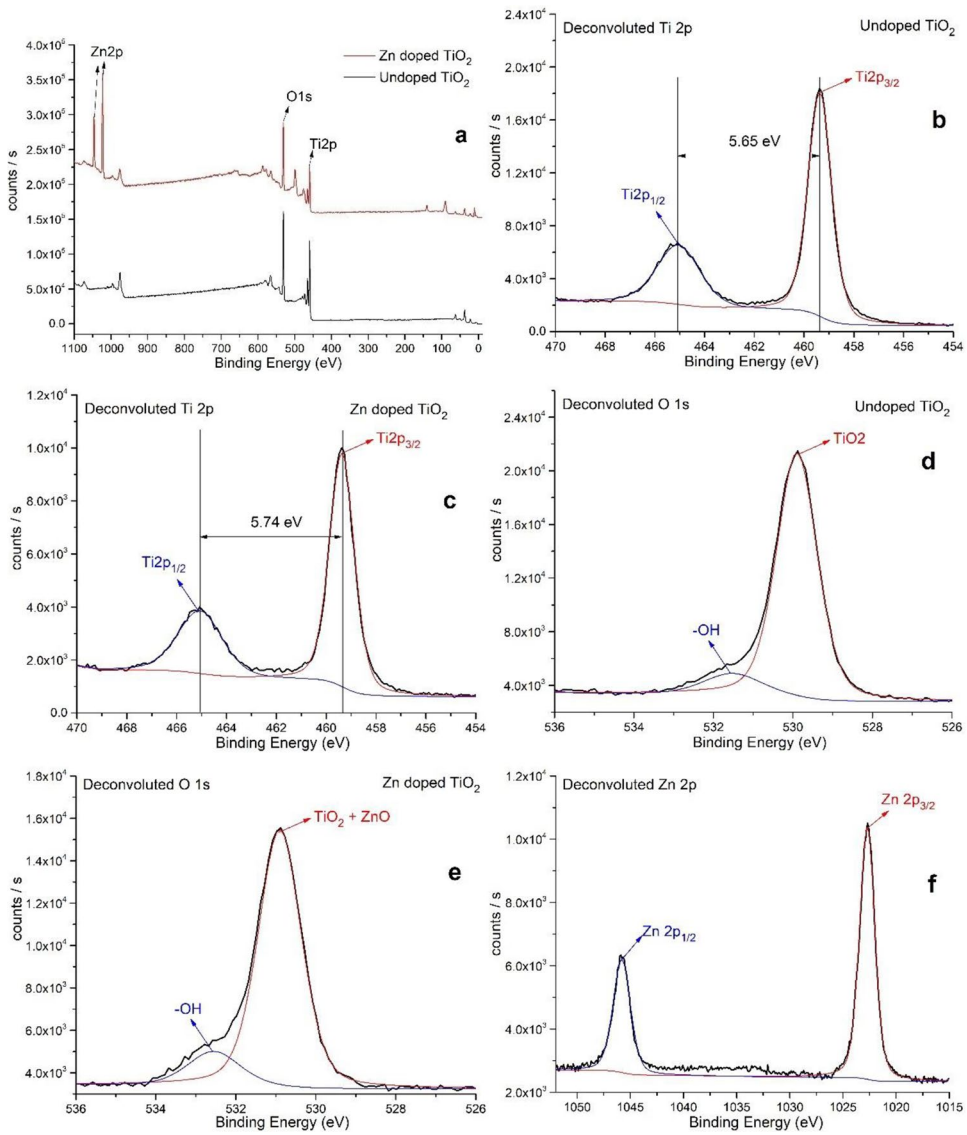

Fig. 4 Survey and high-resolution XPS spectrums of undoped and Zn-doped TiO_2 films

[28, 30]. Consequently, the peaks location derived from XPS spectrum, in conjunction with the lack of oxidized zinc derived from XRD pattern, provides a clear proof of incorporating Zn ions into the TiO_2 lattice all through the doping process.

Table 1 XPS results (binding energy and weight %) of undoped and Zn-doped TiO_2 nanophosphors

Sample name	Elements	Binding energy (eV)			Survey weight (%)
		Survey B.E	Deconv. elemental B.E		
			1. peak	*2. peak*	
Undoped TiO_2	Ti 2p	459.13	459.37	465.02	57.82
	O 1 s	530.98	529.87	531.56	42.18
Zn-doped TiO_2	Ti 2p	459.13	459.36	465.10	28.75
	O 1 s	531.16	530.89	532.57	27.16
	Zn 2p	1022.92	1022.69	1045.80	44.09

Photocatalytic activity

It was observed the photocatalytic properties evaluating the degradation of methylene blue at regular time intervals by measuring the absorbance via a UV–vis spectrophotometer. The time-dependent MB aqueous solution degradation studies were reacted in the presence of undoped TiO_2 and Zn-doped TiO_2 samples. Also, the MB solution without sample was used as a reference for comparison the photocatalytic effectiveness of the prepared photocatalysts. Figure 5 shows the changes in the relative concentration of the MB solution in the presence of photocatalysts under UV–vis light. It can be seen from the Fig. 5 that Zn doping process enhanced the photocatalytic properties of the TiO_2 sample. Furthermore, it was carried out the photocatalytic kinetic experiments to determine the kinetic parameters of the reactions like kinetic rate constant. In order to study the photocatalytic

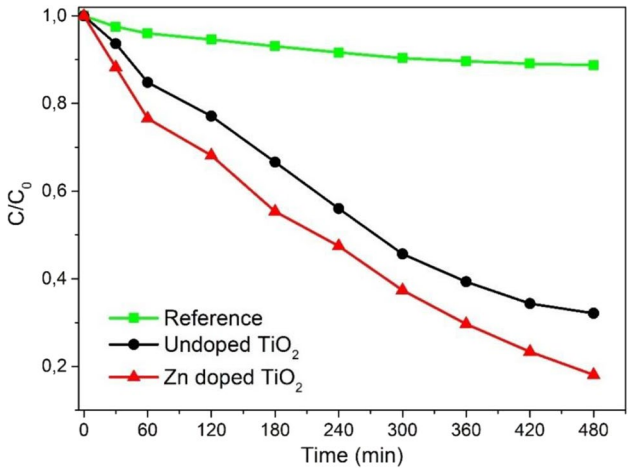

Fig. 5 Photocatalytic degradations of the samples

degradation kinetics of the samples, $\ln(C_0/C) = kt$ equation was utilized. C_0 and C are the original concentration of MB and the corresponding concentration along with the exposure time (t), respectively, and k is the degradation rate constant.

According to Fig. 6, the positive slopes of photocatalytic degradation kinetic of the all samples showed linear behaviour, which followed the pseudo-first-order reaction rate constant. The photocatalytic efficiency values of the undoped TiO_2 and Zn-doped TiO_2 samples were summarized in Table 2. From the Table 2, Zn-doped TiO_2 sample has the highest kinetic constant value which is 0.00342 min^{-1}. It can be clearly seen from the Table 2 that the Zn doping process has caused to increase the photocatalytic performance more than 20% compared to undoped TiO_2 sample.

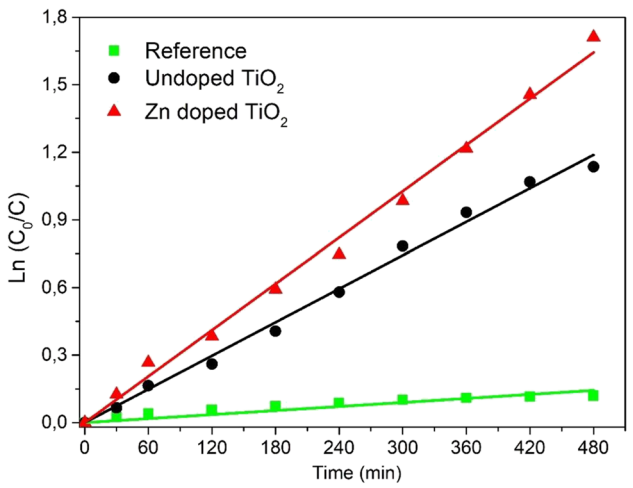

Fig. 6 Photocatalytic kinetic studies of the samples

Table 2 Photocatalytic kinetic parameters of the samples

Sample	Reference	Undoped TiO_2	Zn-doped TiO_2
Degradation efficiency (%)	11.26	67.88	81.93
Reaction rate constant (k) (10^{-4}.min^{-1})	2.98	24.8	34.2
R^2	0.981	0.998	0.998

Conclusion

In summary, Zn-doped TiO_2 films were synthesized by a combination of anodic oxidation and annealing process. Thermal diffusion technique was successfully applied for Zn doping into the TiO_2 lattice. XPS and EDS results proved presence of Zn. SEM micrographs exhibit the morphology of uniformly formed TiO_2 on the Ti substrate. The photocatalytic efficiency values of the undoped TiO_2 and Zn-doped TiO_2 samples were compared by observing degradation rates and kinetic measurements. Zn-doped TiO_2 sample showed remarkably better photocatalytic performance than pure TiO_2. Zn-doped TiO_2 sample has higher kinetic constant value 0.00342 min^{-1}. Degradation efficiency of Zn-doped TiO_2 is 81.93%, while pure TiO_2shows efficiency of 67.88%. The results indicate that the photocatalytic activity of TiO_2 films which obtained anodic oxidation can be enhanced by Zn doping using simple thermal diffusion technique.

Declarations

Conflict of interest The authors declare no competing interests.

References

1. Otero-González, L., García-Saucedo, C., Field, J.A., Sierra-Álvarez, R.: Chemosphere **93**, 1201–1206 (2013)
2. Wang, H., Lewis, J.P.: J. Phys.: Condens. Matter **17**, L209 (2005)
3. Matsui, M., Akaogi, M.: Mol. Simul. **6**, 239–244 (1991)
4. Reed, P.J., Mehrabi, H., Schichtl, Z.G., Coridan, R.H.: ACS Appl. Mater. Interfaces. **10**, 43691–43698 (2018)
5. Xie, Y., Zhao, X., Chen, Y., Zhao, Q., Yuan, Q.: J. Solid State Chem. **180**, 3576–3582 (2007)
6. Li, D., Haneda, H., Hishita, S., Ohashi, N.: Chem. Mater. **17**, 2596–2602 (2005)
7. Romeas, V., Pichat, P., Guillard, C., Chopin, T., Lehaut, C.: Ind. Eng. Chem. Res. **38**, 3878–3885 (1999)
8. Chen, J.S., Tan, Y.L., Li, C.M., Cheah, Y.L., Luan, D., Madhavi, S., Boey, F.Y.C., Archer, L.A., Lou, X.W.: J. Am. Chem. Soc. **132**, 6124–6130 (2010)
9. Kumar, M., Gupta, A.K., Kumar, D.: Ceram. Int. **42**, 405–410 (2016)
10. Gultekin, S., Yildirim, S., Celik, E., Alicikus, L.Z.A.: J. Aust. Ceram. Soc. **54**, 523–531 (2018)

11. Park, N.-G., Van de Lagemaat, J.: Frank, AJ. J. Phys. Chem. B **104**, 8989–8994 (2000)
12. Dargahi, Z., Asgharzadeh, H., Maleki-Ghaleh, H.: Ceram. Int. **44**, 13015–13023 (2018)
13. Demirci, S., Dikici, T., Yurddaskal, M., Gultekin, S., Toparli, M., Celik, E.: Appl. Surf. Sci. **390**, 591–601 (2016)
14. Umebayashi, T., Yamaki, T., Tanaka, S., Asai, K.: Chem. Lett. **32**, 330–331 (2003)
15. Sakthivel, S., Shankar, M., Palanichamy, M., Arabindoo, B., Bahnemann, D., Murugesan, V.: Water Res. **38**, 3001–3008 (2004)
16. Fujishima, A., Honda, K.: Nature **238**, 37–38 (1972)
17. Siemon, U., Bahnemann, D., Testa, J.J., Rodríguez, D., Litter, M.I., Bruno, N.: J. Photochem. Photobiol. A: Chem. **148**, 247–255 (2002)
18. Gao, Y., Lee, W., Trehan, R., Kershaw, R., Dwight, K., Wold, A.: Mater. Res. Bull. **26**, 1247–1254 (1991)
19. Marci, G., Augugliaro, V., Lopez-Munoz, M.J., Martin, C., Palmisano, L., Rives, V., Schiavello, M., Tilley, R.J., Venezia, A.M.: J. Phys. Chem. B **105**, 1033–1040 (2001)
20. Jing, L., Xin, B., Yuan, F., Xue, L., Wang, B., Fu, H.: J. Phys. Chem. B **110**, 17860–17865 (2006)
21. Zhang, W., Zhu, S., Li, Y., Wang, F.: Vacuum **82**, 328–335 (2007)
22. Seo, J.-H., Wu, H., Mikael, S., Mi, H., Blanchard, J.P., Venkataramanan, G., Zhou, W., Gong, S., Morgan, D., Ma, Z.: J. Appl. Physics. **119**, 205703 (2016)
23. George, P., Sanchez, A., Nair, P., Nair, M.: Appl. Phys. Lett. **66**, 3624–3626 (1995)
24. Satta, A., Janssens, T., Clarysse, T., Simoen, E., Meuris, M., Benedetti, A., Hoflijk, I., De Jaeger, B., Demeurisse, C., Vandervorst, W.: J. Vac. Sci. Technol. B: Microelectron. Nanometer Struct. Process. Measure. Phenom. **24**, 494-498 (2006)
25. Huet, K., Mazzamuto, F., Tabata, T., Toque-Tresonne, I., Mori, Y.: Mater. Sci. Semicond. Process. **62**, 92–102 (2017)
26. Gültekin, S., Yıldırım, S., Yılmaz, O., Keskin, İÇ., Katı, M.İ, Çelik, E.: J. Lumin. **206**, 59–69 (2019)
27. Yildirim, S., Yurddaskal, M., Dikici, T., Aritman, I., Ertekin, K., Celik, E.: Ceram. Int. **42**, 10579–10586 (2016)
28. Niaki, A.G., Bakhshayesh, A., Mohammadi, M.: Sol. Energy **103**, 210–222 (2014)
29. Pang, S., Huang, J.g., Su, Y., Geng,B., Lei, S.y., Huang, Y.t., Lyu, C., Liu, X.j.: Photochem. Photobiol. **92**, 651–657 (2016)
30. Zhao, Y., Li, C., Liu, X., Gu, F., Du, H., Shi, L.: Appl. Catal. B **79**, 208–215 (2008)
31. Nair, R.G., Mazumdar, S., Modak, B., Bapat, R., Ayyub, P., Bhattacharyya, K.: J. Photochem. Photobiol., A **345**, 36–53 (2017)
32. Zhang, Y., Wang, L., Liu, B., Zhai, J., Fan, H., Wang, D., Lin, Y., Xie, T.: Electrochim. Acta **56**, 6517–6523 (2011)